Four-dimensional Langevin dynamics of heavy-ion-induced fission

P. N. Nadtochy, E. G. Ryabov, A. E. Gegechkori, Yu. A. Anischenko, and G. D. Adeev
Omsk State University, Mira prospekt 55-A, Omsk 644077, Russia
(Received 4 April 2012; published 25 June 2012)

A four-dimensional dynamical model based on Langevin equations was developed and applied to calculate a wide set of experimental observables for the reactions $^{16}O + ^{208}Pb \rightarrow ^{224}Th$ and $^{16}O + ^{232}Th \rightarrow ^{248}Cf$ over a wide range of excitation energy. The fusion-fission and evaporation residue cross sections, fission fragment mass-energy distribution parameters, prescission neutron multiplicities, and anisotropy of angular distribution of fission fragments could be reasonably reproduced using a modified one-body mechanism for nuclear friction with a reduction coefficient of the contribution from a wall formula $k_s \simeq 0.25$ and a dissipation coefficient for the orientation degree of freedom (K coordinate) $\gamma_K \simeq 0.077$ (MeV zs)$^{-1/2}$. Inclusion of the K coordinate into calculation of potential energy changes the stiffness of the nucleus with respect to mass asymmetry coordinate for the values of $K \neq 0$ and results in a shift of the Businaro-Gallone point towards larger Z^2/A values. The experimental data on the fission fragment mass-energy distribution parameters together with mean prescission neutron multiplicity for heavy fissioning nuclei are reproduced through the four-dimensional Langevin calculations more accurately than through three-dimensional calculations.

DOI: 10.1103/PhysRevC.85.064619 PACS number(s): 25.85.−w, 05.10.Gg, 24.75.+i

I. INTRODUCTION

The dissipative properties of nuclear matter are still a popular subject in experimental and theoretical investigations of the large-amplitude collective motions in nuclei, such as heavy-ion fusion and nuclear fission. Many recent studies have been performed on the basis of one-dimensional [1–4] and multidimensional [5–16] Langevin equations to analyze experimental data on the different features of fusion-fission reactions. All of the above-mentioned applications of Langevin dynamics are used for compound nuclei with zero spin about a symmetry axis, because it was always assumed that angular momentum is not only perpendicular to the reaction plane, but also to the fission direction.

As first pointed out by Lestone in Ref. [17], this assumption is not consistent with statistical model as well as with dynamical treatment of the orientation degree of freedom [18]. Subsequently, Lestone and McCalla introduced the overdamped Langevin equation to describe the dynamical evolution of orientation degree of freedom (K coordinate) and stressed that a large volume of heavy-ion-induced fission data needs to be reanalyzed with dynamical treatment of the orientation degree of freedom [19]. Clearly, consideration of the K coordinate as an independent collective coordinate in multidimensional Langevin dynamics is necessary for dynamical treatment of the fission fragment angular distribution. Yet, in almost all cases, the analysis of the latter is restricted only by the framework of statistical transition-state model. An alternative dynamical description of the evolution of the orientation degree of freedom on the basis of a Metropolis algorithm and an algorithm of Kubo-Anderson process was previously developed in Refs. [20–22]. This approach was successfully applied to describe fragment angular distributions from excited compound nuclei fission.

In the present study, we have performed the extension of the three-dimensional (3D) Langevin dynamical model [23–25] by adding the orientation degree of freedom (K coordinate) to three collective coordinates that describe the shape evolution of the fissioning nucleus. In other words, we are led with a four-dimensional (4D) Langevin model. We have studied the impact of the new additional degree of freedom on observable features of the fission process, such as the parameters of the fission fragment mass-energy distribution (MED), the mean prescission neutron multiplicity, and fusion-fission (FF) and evaporation residue (ER) cross sections. We have also dynamically treated and calculated the angular distribution of fission fragments.

The paper is organized as follows. Section II describes the 4D Langevin model, including its basic equations, input parameters, and details of calculations. Section III presents and discusses the results obtained from the application of the developed model. Finally, Sec. IV contains closing remarks.

II. MODEL

The 4D dynamical model has been constructed on the basis of the 3D model [23–25]. Three collective coordinates are used to describe the shape of the compound nucleus. The fourth collective coordinate is the projection K of the total spin I to the symmetry (elongation) axis of the nucleus. We applied a $\{c, h, \alpha\}$ parametrization [26] of the nuclear shape in the dynamical calculations. The surface of the nucleus in cylindrical coordinates is given by

$$\rho_s^2(z) = \begin{cases} (c^2 - z^2)\left(A_s + Bz^2/c^2 + \frac{\alpha z}{c}\right), & B \geqslant 0; \\ (c^2 - z^2)\left(A_s + \frac{\alpha z}{c}\right)\exp(Bcz^2), & B < 0, \end{cases} \tag{1}$$

where z is the coordinate along the symmetry axis and ρ_s is the radial coordinate of the nuclear surface. In Eq. (1) the quantities B and A_s are defined as

$$B = 2h + \frac{c-1}{2}; \qquad A_s = \begin{cases} c^{-3} - \frac{B}{5}, & B \geqslant 0; \\ -\frac{4}{3}\frac{B}{\exp(Bc^3) + \left(1 + \frac{1}{2Bc^3}\right)\sqrt{-\pi Bc^3}\,\mathrm{erf}\left(\sqrt{-Bc^3}\right)}, & B < 0. \end{cases} \tag{2}$$

In Eqs. (1) and (2), c denotes the elongation parameter, the parameter h describes the variation in the thickness of the neck for a given elongation of the nucleus, and the the mass asymmetry parameter α determines the ratio of the nascent fission fragments volumes.

In the stochastic approach [27–30], evolution of the collective coordinates is considered as motion of Brownian particles which interact stochastically with a large number of internal degrees of freedom, constituting the surrounding "heat bath." The hydrodynamical friction force is assumed to be derived from the random force averaged over a time larger than the collision time scale between collective and internal degrees of freedom. The random part is modeled as a Gaussian white noise which causes fluctuations of the collective variables resulting in fluctuations of the physical observables in fission process. The coupled Langevin equations have the form

$$\begin{aligned}\frac{dq_i}{dt} &= \mu_{ij}p_j,\\ \frac{dp_i}{dt} &= -\frac{1}{2}p_j p_k\frac{\partial\mu_{jk}}{\partial q_i} - \left(\frac{\partial F}{\partial q_i}\right)_T - \gamma_{ij}\mu_{jk}p_k + \theta_{ij}\xi_j(t),\end{aligned} \tag{3}$$

where $\mathbf{q}$ is the vector of collective coordinates, $\mathbf{p}$ is the vector of conjugate momenta, $F(\mathbf{q}, K) = V(\mathbf{q}, K) - a(\mathbf{q})T^2$ is the Helmholtz free energy, $V(\mathbf{q})$ is the potential energy, $m_{ij}(\mathbf{q})$ ($\|\mu_{ij}\| = \|m_{ij}\|^{-1}$) is the tensor of inertia, and $\gamma_{ij}(\mathbf{q})$ is the friction tensor. The $\xi_j(t)$ is a random variable satisfying the relations

$$\langle\xi_i\rangle = 0, \quad \langle\xi_i(t_1)\xi_j(t_2)\rangle = 2\delta_{ij}\delta(t_1 - t_2). \tag{4}$$

Thus, the Markovian approximation is assumed to be valid. The strength of the random force θ_{ij} is given by the Einstein relation $\sum\theta_{ik}\theta_{kj} = T\gamma_{ij}$. The temperature of the "heat bath" T has been determined by the Fermi-gas model formula $T = (E_{\rm int}/a)^{1/2}$, where $E_{\rm int}$ is the internal excitation energy of the nucleus and $a(\mathbf{q})$ is the level-density parameter with the coefficients taken from the work of Ignatyuk and coauthors [31]. It should be stressed that the driving force in an excited system is not simply the negative gradient of the conservative potential $V(\mathbf{q})$ but should contain a thermodynamical correction:

$$Q_i = -\left(\frac{\partial F}{\partial q_i}\right)_T = -\frac{\partial V(\mathbf{q})}{\partial q_i} + \frac{\partial a(\mathbf{q})}{\partial q_i}T^2. \tag{5}$$

Thus in the present study, the Helmholtz free energy is the thermodynamical driving potential [11,24,25,30]. The repeated indices in the equations above imply summation over the collective coordinates.

The three collective coordinates $\mathbf{q} = (q_1, q_2, q_3)$ are related to the shape parameters c, h, and α by $q_1 = c$, $q_2 = (h + 3/2)/(\frac{5}{2c^3} + \frac{1-c}{4} + 3/2)$, and $q_3 = \alpha/(A_s + B)$, if $B \geqslant 0$, or $q_3 = \alpha/A_s$, if $B < 0$. The advantage of using the collective coordinates $\mathbf{q}$ instead of the $\{c, h, \alpha\}$ parameters is discussed in Refs. [25,32].

During a random walk along the Langevin trajectory in the space of the collective coordinates, the energy conservation law is used in the form $E^* = E_{\rm int} + E_{\rm coll} + V + E_{\rm evap}(t)$. Here E^* is the total excitation energy of the nucleus, and $E_{\rm coll} = 0.5\sum\mu_{ij}p_i p_j$ is the kinetic energy of the collective degrees of freedom. The value $E_{\rm evap}(t)$ is the energy carried away by the evaporated particles by the time t. The potential energy of the nucleus was calculated within the framework of a macroscopic model with finite range of the nuclear forces [33] using parameters from Ref. [34]. The potential energy was obtained as a sum of the Coulomb energy, the generalized surface energy (the nuclear interaction energy), and the rotational energy. The inertia tensor was calculated by applying the Werner-Wheeler approximation for incompressible irrotational flow [35].

A modified one-body mechanism of nuclear dissipation [36,37] similar to that proposed in Refs. [38,39] with the use of the center-of-mass motion for the drift velocity and inclusion of the so-called completed "wall-and-window" term introduced by Randrup and Swiatecki [40] was employed to determine the dissipative part of the driving forces. The friction tensor was calculated using the "wall-plus-window" formula for strongly necked-in shapes, while only the "wall" formula contribution was used for compact mononuclear shapes. In the intermediate case for the shapes that are neither compact nor strongly necked-in, a smooth interpolation [41,42] between the "wall" and "wall-plus-window" formula was used with a form factor ranging from 1 for mononuclear-like shapes to 0 for the shapes with zero neck radius. Reduction coefficients $k_s = 0.25$ and $k_s = 0.5$ of contribution from the "wall" formula are used in the present calculations. An explicit expression for the friction tensor is given in Refs. [21,23,42]. The value $k_s = 1.0$ corresponds to the standard "wall" and "wall-plus-window" formulas [36,37,43], whereas values $0.2 < k_s < 0.5$ allow the reproduction of different features of the mass-energy distribution, particle multiplicities in multidimensional Langevin calculations [5,6,11,24,25,42,44], and the widths of isoscalar giant resonances over a broad range of nuclear masses [38]. Furthermore, the necessity of the k_s reduction factor is compatible with other theoretical predictions [45–48].

The description of evolution of the K collective coordinate using the Langevin equation for overdamped motion has been recently proposed in Ref. [19]. Such description is more consistent than the application of the Metropolis algorithm [20,21,49]. The Langevin equation for the K coordinate allows the modeling of the relaxation process of K states depending on the instantaneous physical properties of fissioning system such as temperature and moment of inertia instead of treating the corresponding relaxation time τ_K as a free parameter [20–22]. However, the main drawback of this approach is the lack of detailed description of the coupling between the orientation degree of freedom and the "heat bath." Successful application of the transition-state model of angular distributions to the large number of fusion-fission reactions suggests that K can be treated as an overdamped collective coordinate [19]. This means that the stochastic dynamics of the orientation degree of freedom does not include the inertia parameter and could be described by the overdamped Langevin equation:

$$dK = -\frac{\gamma_K^2 I^2}{2}\frac{\partial V}{\partial K}dt + \gamma_K I\sqrt{\frac{T}{2}}\xi(t), \tag{6}$$

where $\xi(t)$ has the same meaning as in Eq. (3) and γ_K is a parameter controlling the coupling between the orientation degree of freedom K and the "heat bath." As the level density parameter $a(\mathbf{q})$ does not depend on K, the conservative force

in the Langevin Eq. (6) is calculated as a derivative of the potential energy.

The Langevin equations for the shape parameters (3) and the Langevin equation for the K coordinate (6) are connected through the potential energy. The Langevin dynamics of the K coordinate is influenced by the actual value of potential energy $V(\mathbf{q}, I, K)$. At the same time, the rotational part of the potential energy is dependent on the actual K value at time t, and this way it influences the dynamical evolution of shape parameters.

The rotational part of the potential energy is determined by the expression

$$E_{\rm rot}(\mathbf{q}, I, K) = \frac{\hbar^2 K^2}{2J_{\parallel}(\mathbf{q})} + \frac{\hbar^2[I(I+1) - K^2]}{2J_{\perp}(\mathbf{q})} = \frac{\hbar^2 I(I+1)}{2J_{\perp}(\mathbf{q})} + \frac{\hbar^2 K^2}{2J_{\rm eff}(\mathbf{q})}. \quad (7)$$

The functionals $J_{\parallel}$ and $J_{\perp}$ are the rigid body moments of inertia, about and perpendicular to the symmetry axis. To account for the diffuseness of the nuclear surface, moments of inertia should be calculated as follows [50]:

$$J_{\perp(\parallel)}(\mathbf{q}) = J^{(\rm sharp)}_{\perp(\parallel)}(\mathbf{q}) + 4M_0 a_M^2, \quad (8)$$

where $a_M = 0.704$ fm is the diffuseness parameter of the nuclear surface, M_0 is the compound nucleus mass, and $J^{(\rm sharp)}_{\perp(\parallel)}$ are the moments of inertia for a sharp-edged nuclear density distribution. The effective moment of inertia is $J^{-1}_{\rm eff} = J^{-1}_{\parallel} - J^{-1}_{\perp}$. The expressions for the $J^{(\rm sharp)}_{\perp(\parallel)}$ in the $\{c, h, \alpha\}$ parametrization could be found in Ref. [51].

Based on the works of Døssing and Randrup [52,53], Lestone and McCalla [18,19] have shown that in the case of a dinucleus γ_K can be expressed as

$$\gamma_K = \frac{1}{R_N R_{\rm c.m.}\sqrt{2\pi^3 n_0}}\sqrt{\frac{J_{\parallel}|J_{\rm eff}|J_R}{J^3_{\perp}}}, \quad (9)$$

where R_N is the neck radius, $R_{\rm c.m.}$ is the distance between the centers of mass of the nascent fragments, n_0 is the bulk flux in standard nuclear matter (0.0263 MeV zs fm^{-4}) [53], and $J_R = M_0 R^2_{\rm c.m.}/4$ for a reflection-symmetric shape. In a limiting case $\gamma_K \to 0$ and with an initial K value equal to zero, the present 4D Langevin model is reduced to the 3D model [23–25].

The deformation dependence of the dissipation coefficient γ_K given by Eq. (9) should be used with caution as is stated in Ref. [19], because Eq. (9) was obtained assuming nuclear shapes featuring a well-defined neck. Therefore, following Ref. [19], we choose γ_K to be a constant equal to 0.077 (MeV zs)$^{-1/2}$. This estimation has been obtained using Eq. (9) for elongated nuclear shapes featuring a neck, which corresponds to the deformations typical for the descent from saddle to scission point. The above-mentioned value of the friction parameter γ_K used in Refs. [17,19] was obtained by Lestone and coauthors in their early study [54] from an analysis of fission fragment angular distribution measured for a number of fusion-fission reactions. This value was further used in Refs. [17,19] in calculations of the mean fission time of compound excited nuclei. Since this estimate may be incorrect by a factor of 2 or more [19], we also performed calculations with different γ_K values, trying to explore the sensitivity of observables to the k_s and γ_K parameters.

Evaporation of prescission light particles (n, p, α, γ) along Langevin fission trajectories was taken into account using a Monte Carlo simulation technique [55]. The angular momentum L for each Langevin trajectory has been sampled from the spin distribution function

$$\sigma(L) = \frac{2\pi}{k^2}\frac{2L+1}{1+\exp[(L-L_c)/\delta L]}, \quad (10)$$

where k, L_c, and δL are the wave number, critical angular momentum for fusion, and diffuseness, respectively. In the first approximation, L_c and δL values were defined according to the scaled prescription [30], which reproduces to a certain extent the dynamical results of the surface friction model [56] for fusion of two heavy ions. Finally, the quantities L_c and δL were constrained from the experimental fusion cross section and $\langle L^2\rangle$. In the present study, we neglected the spins of projectile and target nuclei and assumed that the spin of the compound nucleus $I \simeq L$. The initial K value was generated using the Monte Carlo method from uniform distribution in the interval $(-L, L)$ [19,20]. The initial conditions for the shape coordinates were chosen as follows. We started modeling fission dynamics from the spherical compound nucleus, i.e., $\mathbf{q}_0 = (q_{10} = 1.0, q_{20} = 0.375, q_{30} = 0.0)$, with thermalized internal degrees of freedom. It was supposed that the scission occurred when the neck radius of the fissioning nucleus was equal to $0.3R_0$ [26,57] (R_0 is the radius of the initial spherical nucleus). This scission condition determines the scission surface in the multidimensional space of collective coordinates. The Langevin trajectory determines the shape of the fissioning nucleus at the moment of scission into fragments by crossing the scission surface. The dynamical trajectory will either reach the scission surface, in which case it is counted as a fission event, or if the excitation energy for a trajectory which is still inside the saddle reaches the value $E_{\rm int} + E_{\rm coll}(\mathbf{q}, \mathbf{p}) < \min(B_j, B_f)$, the event is counted as an evaporation residue (B_j is the binding energy of the particle $j = n, p, \alpha, \gamma$). The dynamical Eqs. (3) and (6) were integrated simultaneously with the same time step until the scission or evaporation residue condition occurs. Correspondingly, the ensemble of sampled Langevin trajectories determines the ensemble of fission fragments and evaporation residue nuclei, and one can obtain the observables of interest, typical for FF or ER channels, such as masses and kinetic energies of fission fragments, K values, and temperatures.

In the standard theoretical approach, fission fragments are assumed to be emitted along the direction of the nuclear symmetry axis at the transition state configuration. The angular distribution in this case is given by Refs. [58,59]

$$W(\theta, I, K) = (I + 1/2)|D^I_{M,K}(\theta)|^2, \quad (11)$$

where quantum number M is the projection of the total spin I on the space-fixed axis, θ is the angle with respect to the space-fixed axis, and $D^I_{M,K}(\theta)$ is the symmetric-top wave function. In case of zero spin target and projectile nuclei, M is zero, and the angular distribution of fission fragments is determined by averaging the expression (11) over ensemble of Langevin

trajectories

$$W(\theta) = \frac{1}{N_f}\sum_{j=1}^{N_f}(I^j + 1/2)\left|D^{I^j}_{0,K^j}(\theta)\right|^2, \tag{12}$$

where upper index j determines the value of corresponding quantity at the scission point for the jth Langevin trajectory and N_f is the number of trajectories reaching the scission surface. Applying Eq. (12) within the present 4D calculations we determine the angular distribution at the scission surface. This procedure does not use the assumptions of the standard transition-state model, as the K distribution is determined dynamically at every time step. Thus, there is no need of any assumption of its distribution at any arbitrary transition point.

Additionally, the standard transition-state model has been used to analyze fission fragment angular distributions. These calculations have been performed to compare the predictions of widely used transition-state models with the present dynamical model. In the transition-state model, the equilibrium distribution over the K degree of freedom is assumed to be established at the transition state. Usually two limiting assumptions on the position of the transition state and, correspondingly, two versions of the transition-state theory exist: the saddle-point transition-state (SPTS) [58] and the scission-point transition-state (SCTS) [60] models. We use the last passage of the saddle point by the fissioning system [13] in the case of the SPTS model to find observables of interest. In the case of the multidimensional model, a set of relevant conditional saddle or scission points plays the role of transition states. A frequently used approximation to the fission fragment angular distributions involves a computation of the following expression:

$$W(\theta, I) = \frac{(2I+1)\exp[-p\sin^2\theta]J_0[-p\sin^2\theta]}{\mathrm{erf}\,[\sqrt{2p}\,]}, \tag{13}$$

where J_0 is the zeroth-order Bessel function, $p = (I + \frac{1}{2})^2/(4K_0^2)$, and the variance of the equilibrium K distribution K_0 is

$$K_0^2 = J_{\mathrm{eff}}T/\hbar^2. \tag{14}$$

Here T and J_{eff} are taken at the transition state. We explicitly take into account the dependence of transition-state deformation on the I value. One must sum the expression (13) over I to obtain the angular distribution:

$$W(\theta) = \sum_{I=0}^{\infty}\sigma(I)W(\theta, I). \tag{15}$$

The anisotropy of the fission fragment angular distribution is then given by

$$A = \frac{W(0^\circ)}{W(90^\circ)}, \tag{16}$$

where angular distribution $W(\theta)$ could be found either from 4D calculations using Eq. (12) or from the equilibrium K distribution at transition state using Eqs. (13)–(15).

Three quantities determine the angular distribution in the transition-state model: the initial spin distribution of compound nuclei, the effective moment of inertia, and the nuclear temperature at the transition state. In the case of $p \gg 1$ [see Eq. (13)], the anisotropy of the angular distribution is given by the approximate relation

$$\frac{W(0^\circ)}{W(90^\circ)} \simeq 1 + \frac{\langle I^2\rangle}{4K_0^2}. \tag{17}$$

Note that the K distribution obtained from 4D dynamical calculations will be identical to the equilibrium K distribution at the saddle point for the case in which the relaxation time of the K degree of freedom τ_K is shorter than the time spent by the nucleus near the saddle point and larger than the time of descent from saddle to scission point. If, on the contrary, the τ_K is much shorter than the descent time from saddle to scission point, the dynamically calculated K distribution will be similar to the equilibrium K distribution at the scission point. In the present dynamical calculations, we do not use any approximation about the relaxation time for the K coordinate. Instead, we directly treat the relaxation process of the K coordinate using Eq. (6) and take into account the influence of the actual evolution of the K value on the dynamics of the shape parameters (q_1, q_2, q_3).

The analysis of the ensemble-averaged Eq. (6) leads to the expression for the K-state relaxation time

$$\frac{d\langle K\rangle}{dt} = -\frac{\gamma_K^2 I^2}{2}\left\langle\frac{\partial V}{\partial K}\right\rangle. \tag{18}$$

From the expression for the rotational energy, it follows that

$$\frac{d\langle K\rangle}{dt} = -\frac{\gamma_K^2 I^2}{2}\frac{\hbar^2}{J_{\mathrm{eff}}}\langle K\rangle. \tag{19}$$

Assuming a constant γ_K, as we do in the present study, the solution of this equation has the form

$$\langle K(t)\rangle_{K_0} = K_0\exp\left[-\frac{\gamma_K^2 I^2\hbar^2}{2J_{\mathrm{eff}}}(t - t_0)\right], \tag{20}$$

which gives the following expression for the relaxation time:

$$\tau_K = \frac{2J_{\mathrm{eff}}}{\gamma_K^2 I^2\hbar^2}. \tag{21}$$

Another estimate for τ_K can be found in Ref. [61]:

$$\tau_K = \frac{C_K J_\perp^2}{t[I(I+1) - K^2]\hbar^2}. \tag{22}$$

It is based on the ideas of Randrup and Døssing [62]. Here C_K is a coefficient that was varied to describe experimental data more precisely.

III. RESULTS AND DISCUSSION

We performed calculations for the compound nuclei ^{224}Th and ^{248}Cf formed in the following heavy-ion reactions:

(i) $^{16}\mathrm{O} + {}^{208}\mathrm{Pb} \rightarrow {}^{224}\mathrm{Th}$ ($E_{\mathrm{lab}} = 90$, 110, 130, 148, and 215 MeV) [63–72];

(ii) $^{16}\mathrm{O} + {}^{232}\mathrm{Th} \rightarrow {}^{248}\mathrm{Cf}$ ($E_{\mathrm{lab}} = 90$, 95, 120, 140, and 160 MeV) [72–76].

These reactions have been studied experimentally and extensive experimental observables are available for the comparison

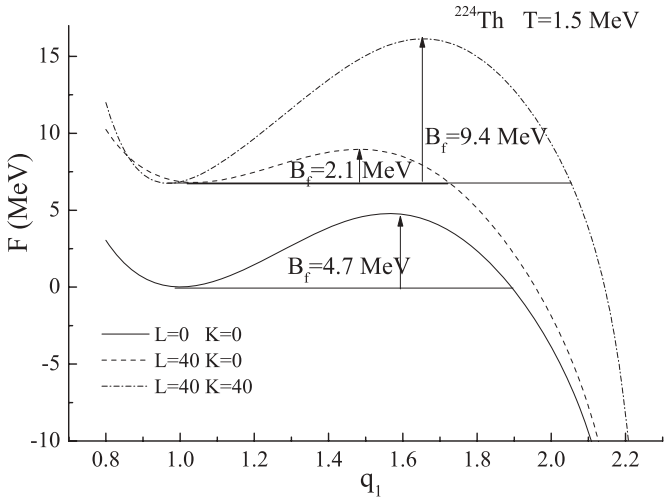

FIG. 1. The Helmholtz free energy along the mean fission trajectory for the ^{224}Th compound nucleus as the function of the elongation parameter q_1, and corresponding fission barriers (B_f) for different combinations of L and K values.

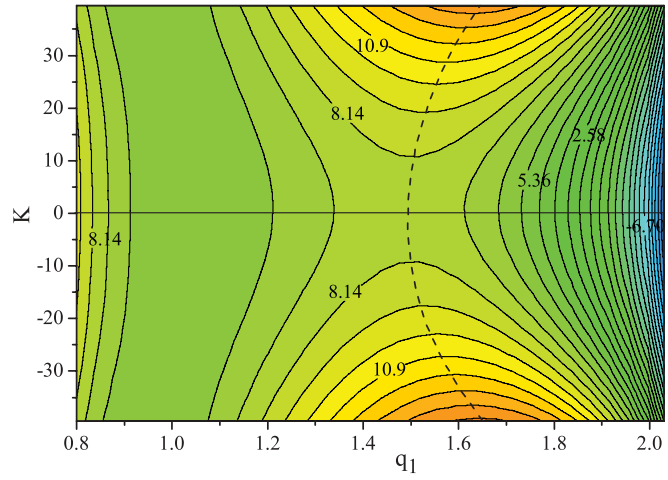

FIG. 2. (Color online) The Helmholtz free energy for the compound nucleus ^{224}Th in the collective coordinates q_1 and K at $T = 1.5$ MeV. The parameters h and α are fixed and equal to zero. The numbers at the contour lines indicate the Helmholtz free energy values in MeV. The dashed curve shows the dependence of saddle-point deformations on K.

with theoretical predictions. In the present analysis, we consider only two compound nuclei and do not attempt to get the best fit of all available experimental data as we mainly explore the effects related to the extension of our model from 3D to 4D, by the explicit dynamical treatment of the K orientation degree of freedom.

A. Influence of the K coordinate on the driving potential

We will start our analysis with static influence of the K coordinate on the driving potential landscape and then briefly discuss dynamic aspects. The crucial changes of potential energy come from rotational energy. The latter increases the fission barrier height for the values $K \neq 0$ [19,77]. The example of the Helmholtz free energy potential along the fission path for ^{224}Th is shown in Fig. 1 for different combinations of L and K values. A substantial increase of fission barrier could be obtained at large angular momenta, whenever K is different from zero. Such increase of fission barrier will reduce the fission rate (increase the mean fission time) and increase the number of evaporated prescission particles. This effect is qualitatively equivalent to the increase of the dissipation strength in 3D calculations. Therefore, it is expected that in 4D calculations a lower value of dissipation strength will result in similar fission probabilities and prescission particles multiplicities as does a larger dissipation coefficient in 3D calculations. Specifically, the inclusion of the K coordinate changes not only the fission barrier height, but it affects also the saddle-point configuration as seen in Figs. 1 and 2.

The landscape of the Helmholtz free energy as a function of collective coordinates q_1 and K is presented in Fig. 2, which also shows the change of the saddle-point deformations with increase of K value. In addition the figure illustrates the range of K values potentially available to the fissioning nucleus. We further present in Fig. 3 the dependence of saddle-point quadrupole moments on the K coordinate for a wide set of beta-stable nuclei. Large K values affect the saddle-point quadrupole moments of light and heavy nuclei in opposite directions.

The rotational energy decreases the stiffness (stability) of nuclei with respect to the mass asymmetry deformations $d^2F/d\eta^2$ for the values $K \neq 0$. Here $\eta = 2(M_1 - M_2)/(M_1 + M_2)$ is the mass asymmetry coordinate introduced by Strutinsky [78], where M_1 and M_2 are the fission fragment masses. The coordinate η is key in analysis of fission fragment mass distribution [79]. The $d^2F/d\eta^2$ values along the mean fission trajectory are shown in Fig. 4 for the nucleus ^{224}Th. The stiffness of the nucleus with respect to the mass asymmetry

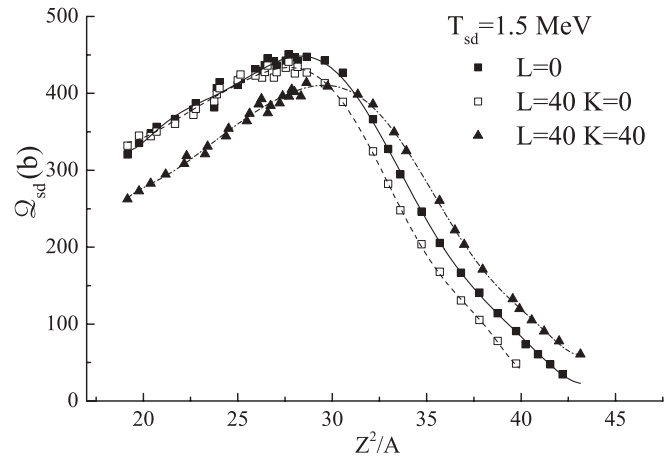

FIG. 3. Quadrupole moments of the saddle-point configurations $\mathcal{Q}_{sd}$ (in barns) as a function of the parameter Z^2/A for beta-stable nuclei at nuclear temperature $T_{sd} = 1.5$ MeV. The solid curve corresponds to the polynomial approximation of the calculated data for a nonrotating nucleus ($L = 0$). Dash and dash-dotted curves are polynomial approximations of the results obtained for $L = 40$ with $K = 0$ and $K = L = 40$, respectively.

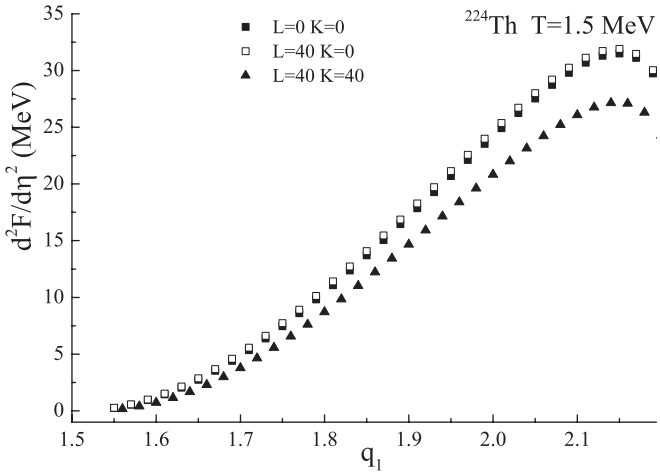

FIG. 4. The stiffness of the free energy landscape for the ^{224}Th compound nucleus with respect to the mass asymmetry coordinate η along the mean fission trajectory as a function of the elongation parameter q_1. Different combinations of L and K are considered as indicated.

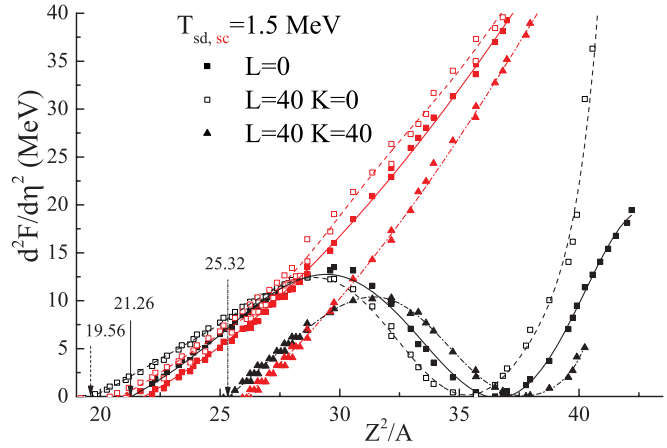

FIG. 5. (Color online) The stiffness of the beta-stable nuclei with respect to mass asymmetry coordinate at the saddle (black symbols and curves) and scission (red symbols and curves) points, $d^2F/d\eta^2$ (in MeV), for nuclei along the beta-stability line at temperature $T = 1.5$ MeV. The solid curves correspond to the polynomial approximation for the calculated data for the non-rotating nucleus ($L = 0$). Dashed and dash-dotted curves are polynomial approximations for the $L = 40$ and $K = 0$ and $K = L = 40$ cases respectively. The arrows with the numbers indicate the corresponding Businaro-Gallone point for each pair of L and K.

$d^2F(K \neq 0)/d\eta^2$ is lower than $d^2F(K = 0)/d\eta^2$ for all deformations with $q_1 > 1.55$, which correspond to the descent from saddle to scission point. This lowering directly comes from the inclusion of the K coordinate, as $d^2F(L = 0, K = 0)/d\eta^2$ and $d^2F(L = 40, K = 0)/d\eta^2$ are substantially higher than $d^2F(L = 40, K = 40)/d\eta^2$. The difference between $d^2F(L = 0, K = 0)/d\eta^2$ and $d^2F(L = 40, K = 40)/d\eta^2$ increases with deformation, and the difference reaches 10% for the compound nucleus ^{248}Cf and 12% for ^{224}Th at the scission point configurations respectively. The increase of angular momentum L only slightly increases the stiffness of the nucleus with respect to mass asymmetry, whereas increase of K decreases it more notably. This decreasing of compound nucleus stability with respect to mass asymmetry coordinate after inclusion of K coordinate should make the mass distribution of fission fragments broader with respect to the 3D calculations, where $K = 0$ is supposed during the fission process.

In the present analysis, we investigated the behavior of $d^2F(L, K)/d\eta^2$ at saddle and scission points for a wide set of beta-stable nuclei and the results are presented in Fig. 5. The main changes of stiffness at both saddle and scission points $[d^2F(L, K)/d\eta^2]_{\mathrm{sd,sc}}$ are caused by the inclusion of the K coordinate for all considered nuclei in the range $20 < Z^2/A < 42$. The increase of K qualitatively results in a parallel shift of the $[d^2F(L, K)/d\eta^2]_{\mathrm{sd,sc}}$ curves presented in Fig. 5 towards larger Z^2/A values. Hence, the Businaro-Gallone point moves from approximately $Z^2/A \simeq 20$ for the case of $K = 0$ to the $Z^2/A \simeq 25$ for the case of $L = K = 40$. Another sizable effect is the substantial decrease of mass asymmetry stiffness $[d^2F(L, K)/d\eta^2]_{\mathrm{sd}}$ at the saddle point for the heavy nuclei with $Z^2/A \simeq 40$. The value of $[d^2F(L = 40, K = 40)/d\eta^2]_{\mathrm{sd}}$ is around 5 times smaller than $[d^2F(L = 40, K = 0)/d\eta^2]_{\mathrm{sd}}$. Therefore, for the heavy compound nuclei considered in the present paper the inclusion of the K coordinate should increase the width of the mass distribution.

The impact of K state on the shape degrees of freedom can be estimated based on the expressions for the Helmholtz free energy and rotational energy (7). The difference between driving forces for the ith shape collective coordinate in 4D and 3D cases can be expressed as

$$Q_i^{(4D)} - Q_i^{(3D)} = -\frac{\partial}{\partial q_i}\frac{\hbar^2 K^2}{2J_{\mathrm{eff}}} = \frac{\hbar^2 K^2}{2J_{\mathrm{eff}}^2}\frac{\partial J_{\mathrm{eff}}}{\partial q_i}. \qquad (23)$$

Considering the one-dimensional case of elongation coordinate q_1, the effective moment of inertia decreases as the nucleus elongates from the ground state to scission; thus the derivative in the expression above is negative. This means that the driving force in fission direction in 4D is weaker than the one in 3D, which in turn leads to smaller fission rates and, correspondingly, to larger mean fission times [80–82].

Despite the well-determined static influence of the K coordinate, these effects will provide complicated interplay between each other in dynamical calculations with varying K value. Thus the quantitative influence of the K coordinate dynamics on the results of 4D calculations for different observables with respect to the 3D case is difficult to predict.

B. Dynamical observables

1. *Cross sections, parameters of the fission fragment MED, and the mean prescission neutron multiplicity*

Different fission characteristics of the heavy compound nuclei ^{224}Th and ^{248}Cf produced, respectively, in the reactions ^{16}O + ^{208}Pb and ^{16}O + ^{232}Th have been intensively investigated experimentally [63–76] and theoretically [20,23,24,44,71,83]. The results of 3D Langevin calculations [23,24,44] demonstrated that a simultaneous reproduction of the width

of fission fragment mass distribution and mean prescission neutron multiplicity for heavy fissioning nuclei is difficult. To reproduce the fission fragment MED parameters, $k_s \simeq 0.1$ should be used. On the contrary, to reproduce the mean prescission neutron multiplicity, large dissipation coefficient $k_s \simeq 1$ needs to be employed. This inconsistency was particularly strong for the heavy fissioning nucleus ^{260}Rf [23]. A similar result for the mean prescission neutron multiplicity was obtained in Ref. [84], where it was shown that the k_s value should range from 4 to 12 to reproduce the data for the compound nuclei with $A_{\rm CN} > 260$.

The present 4D calculations will illustrate that the inclusion of the K coordinate in the dynamical treatment solves this discrepancy and helps reproduce the mean prescission neutron multiplicity and the width of the fission fragment mass distribution with a unified k_s value. The K coordinate increases the fission barrier height and decreases the stiffness of the nucleus with respect to the mass asymmetry coordinate $d^2F/d\eta^2$. The higher fission barrier will increase the fission time and, as a result, increase the number of evaporated particles during the fission process. On the other hand, the decrease of the mass asymmetry stiffness of the nucleus should increase the width of mass distribution.

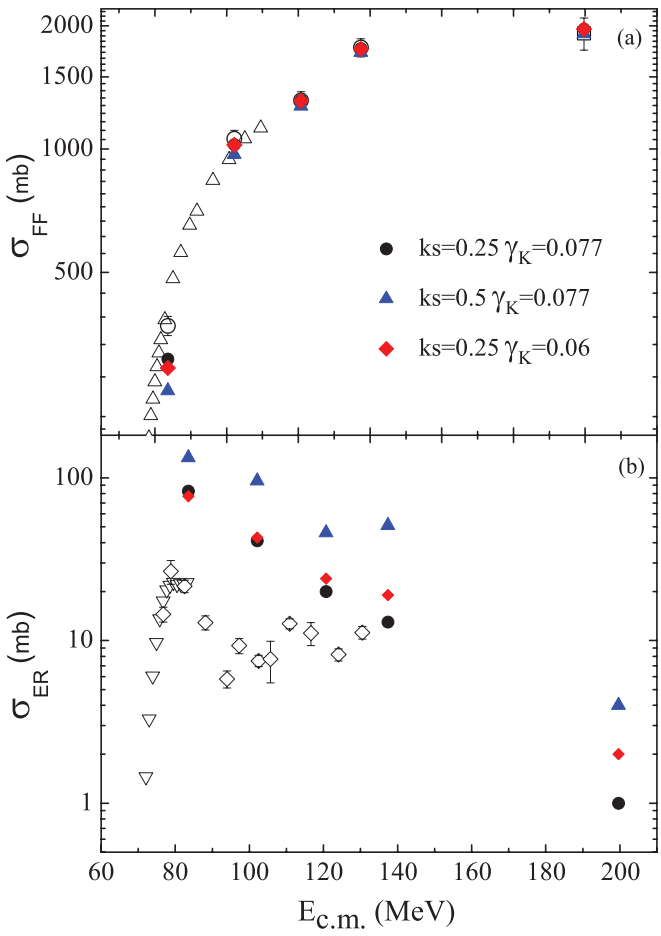

FIG. 6. (Color online) The fusion-fission $\sigma_{\rm FF}$ (a) and evaporation residues $\sigma_{\rm ER}$ (b) cross sections for the compound nucleus ^{224}Th as a function of center-of-mass energy. The open symbols are experimental data: Ref. [67] (triangles), Ref. [72] (circles), Ref. [64] (diamonds), and Ref. [63] (inverted triangles). The filled symbols are the calculated results with $k_s = 0.25$ and $\gamma_K = 0.077$ (MeV zs)$^{-1/2}$ (circles), with $k_s = 0.25$ and $\gamma_K = 0.06$ (MeV zs)$^{-1/2}$ (diamonds), and with $k_s = 0.5$ and $\gamma_K = 0.077$ (MeV zs)$^{-1/2}$ (triangles).

Our results calculated through the 4D model are summarized in Figs. 6–13 together with the experimental data. In Fig. 6, the fusion-fission and evaporation residue cross sections are presented for the ^{224}Th compound nucleus. The comparison between the results of 4D calculations with experimental data demonstrates that both cross sections could be reproduced quite reasonably at high excitation energy. An overestimation (underestimation) of ER (FF) cross section is obtained at $E_{\rm c.m.} = 80$–120 MeV. This discrepancy at low energies is even higher than in the 3D calculations reported in Ref. [24]. The growth of $\sigma_{\rm ER}$ in 4D in comparison with 3D is contingent upon the growth of fission barrier height after the inclusion of the K coordinate. The level density parameter could further be adjusted to fit experimental $\sigma_{\rm FF}$ and $\sigma_{\rm ER}$. This could suppress evaporation of the particles favoring the FF channel with respect to the ER one. This will decrease $\sigma_{\rm ER}$ and increase $\sigma_{\rm FF}$ leading to a more accurate reproduction of experimental cross sections at low excitation energies. However, we did not endeavor to get a better quantitative description of $\sigma_{\rm ER}$ in our 4D calculations, because a reasonable agreement between theoretical results and experimental data for more complete set of observables could be achieved within the explored ranges of k_s and γ_K (see further below).

The growth of prescission neutron multiplicity is another consequence of extending our model from 3D to 4D. Figure 7 shows that the lower limit of experimental data could be approached even with $k_s = 0.25$, whereas the results of 3D calculations [24] required values of $k_s \geqslant 1$ for the best reproduction of n_{pre} for this nucleus.

In Fig. 8, the variances of the fission fragment mass σ^2_M and kinetic energy $\sigma^2_{E_K}$ distributions are presented in comparison with experimental data. The σ^2_M values calculated in the 4D model are around 50% larger than in 3D case [24]. This

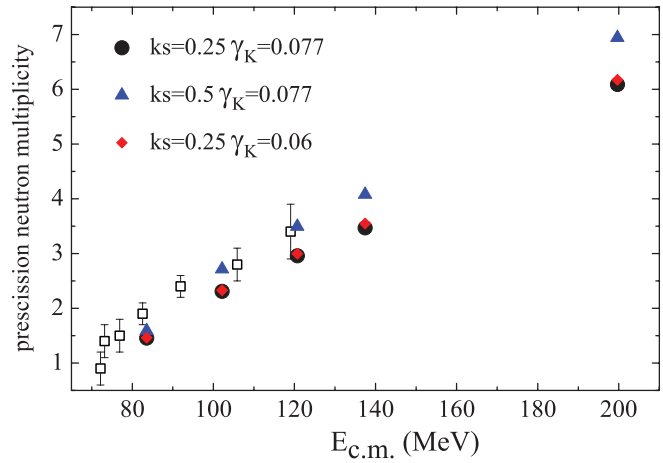

FIG. 7. (Color online) The prescission neutron multiplicity for the compound nucleus ^{224}Th as a function of center-of-mass energy. The open symbols are experimental data from Ref. [71]. The filled symbols are the calculated results with different values of k_s and γ_K, which are marked with the same symbols as in Fig. 6.

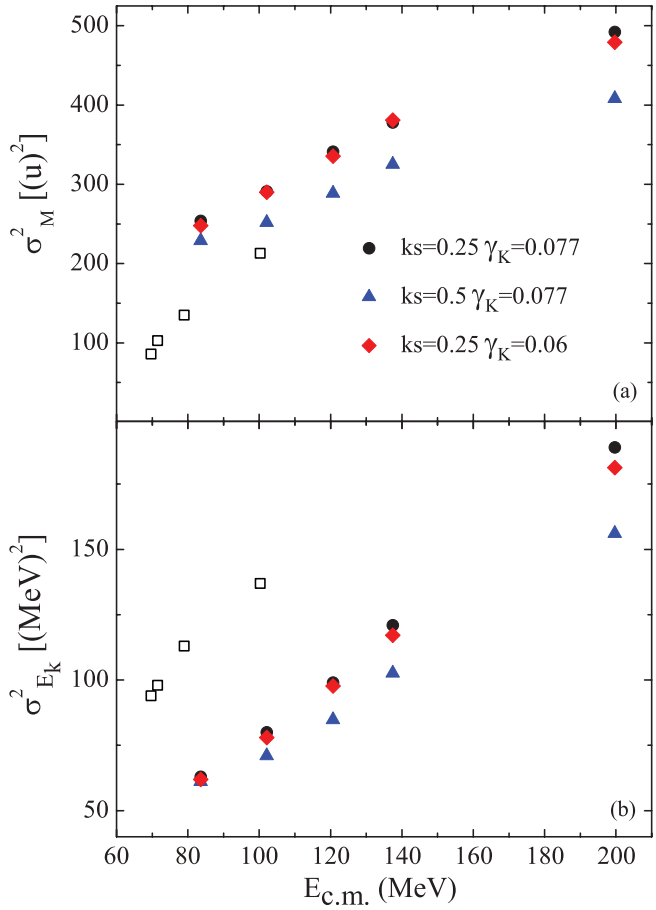

FIG. 8. (Color online) The σ_M^2 (a) and $\sigma_{E_K}^2$ (b) for the compound nucleus ^{224}Th as a function of center-of-mass energy. The open symbols are experimental data from Ref. [70]. The filled symbols are the calculated results with different values of k_s and γ_K, as in Fig. 6.

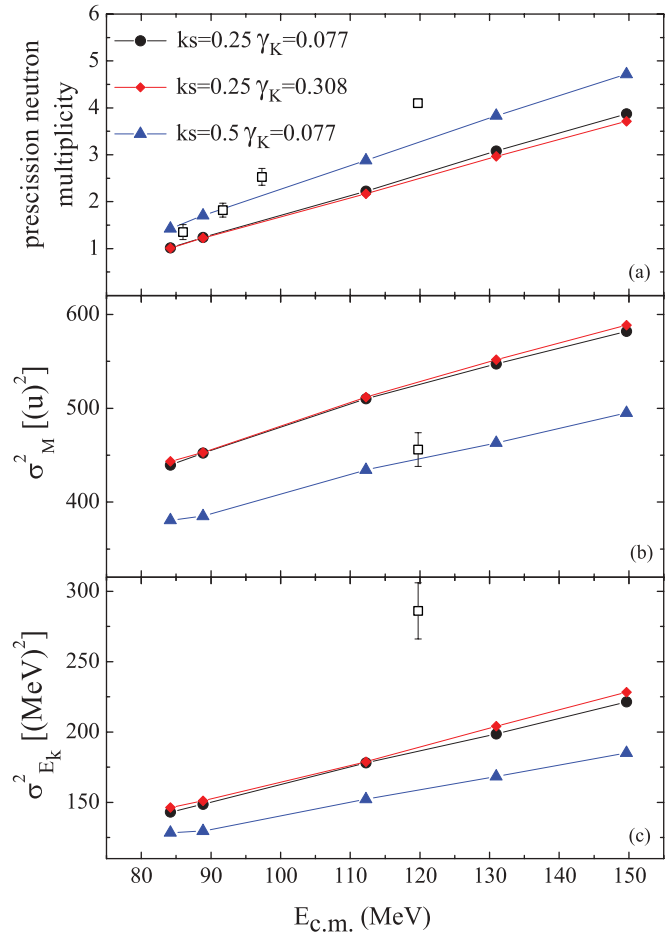

FIG. 9. (Color online) The prescission neutron multiplicity (a), σ_M^2 (b), and $\sigma_{E_K}^2$ (c) for the compound nucleus ^{248}Cf as a function of center-of-mass energy. The open symbols are experimental data from Refs. [73,74]. The filled symbols are the calculated results with $k_s = 0.25$ and $\gamma_K = 0.077$ (MeV zs)$^{-1/2}$ (circles), with $k_s = 0.25$ and $\gamma_K = 0.308$ (MeV zs)$^{-1/2}$ (diamonds), and with $k_s = 0.5$ and $\gamma_K = 0.077$ (MeV zs)$^{-1/2}$ (triangles).

increase is mainly the result of the K coordinate impact on the stiffness of the nucleus $d^2F/d\eta^2$. The calculated σ_M^2 values in 4D with $k_s = 0.25$ and 0.5 overestimate the data by about 50% and 20%, respectively. At the same time, 3D calculations with $k_s = 0.5$ were about 20% lower than experimental values [24]. The agreement between experiment and 4D calculations for the mass width can be further improved by the inclusion of a curvature term in the calculation of the potential energy, as shown in Ref. [85]. Accounting for curvature effects increases the stiffness of the nucleus with respect to mass asymmetry coordinate $d^2F/d\eta^2$ and reduces the width of the mass distribution.

The calculated $\sigma_{E_K}^2$ values stay approximately the same in 3D and 4D calculations. The underestimation of $\sigma_{E_K}^2$ in dynamical calculations is apparently due to a poor ensemble of scission configurations generated by the $\{c, h, \alpha\}$ parametrization [86,87] that does not contain the nuclear shapes with elongated and thick neck, as parametrizations used in Refs [88–90].

In Fig. 9, the σ_M^2, $\sigma_{E_K}^2$, and prescission neutron multiplicity are presented for the compound nucleus ^{248}Cf. Similar conclusions could be drawn from the present 4D results for ^{248}Cf in comparison with the 3D results [24], as could be for the ^{224}Th compound nucleus. The lower values of k_s in the 4D calculations allow the reproduction of the experimental prescission neutron multiplicities, that meets a more complete description of experimental observables in 4D calculations than in 3D. The predicted values of σ_M^2 are larger in 4D calculations than in 3D ones, and the calculated values of $\sigma_{E_K}^2$ underestimate the experimental data.

Figs. 6–9 demonstrate that the dissipation coefficient γ_K influences only slightly the $\sigma_{\rm FF}$ and $\sigma_{\rm ER}$ cross sections, MED parameters, and prescission neutron multiplicity. This could be explained by the fact that the K coordinate affects the evolution of the collective shape coordinates through the sole rotational energy.

2. *The angular distribution of fission fragments*

The observable determined by the dynamical evolution of the K coordinate is the angular distribution. The calcu-

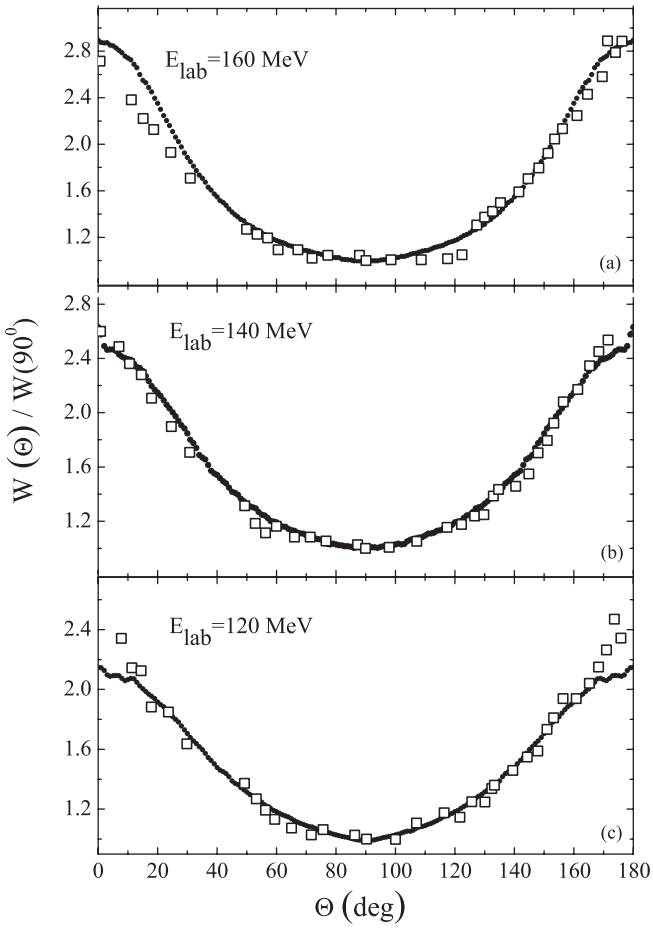

FIG. 10. The fission fragment angular distributions for the compound nucleus ^{248}Cf at $E_{\rm lab} = 120$ (a), 140 (b), and 160 (c) MeV. The open symbols are experimental data from Ref. [72] and the solid circles are results of 4D calculations with $k_s = 0.25$ and $\gamma_K = 0.077$ (MeV zs)$^{-1/2}$.

lated angular distributions for the nucleus ^{248}Cf at different excitation energies are presented in Fig. 10 together with experimental data. This figure illustrates that calculated results adequately fit the experimental data. As mentioned earlier, traditionally the angular distribution is characterized by an anisotropy $A = W(0°)/W(90°)$. The calculated A values for the compound nuclei ^{248}Cf and ^{224}Th are presented in Figs. 11 and 12. In these figures, the results of 4D calculations with different k_s and γ_K values are shown together with the results of the transition-state model implemented at either the saddle or the scission point following Eqs. (13)–(16). The $J_{\rm eff}$ and T at the transition state (saddle or scission point) obtained from the calculations with $k_s = 0.25$ and $\gamma_K = 0.077$ (MeV zs)$^{-1/2}$ were used in order to find the variance K_0^2 of the equilibrium K distribution. The increase of k_s results in an increase of angular anisotropy, as found in 3D calculations [11,24], where a detailed analysis of the influence of k_s and dimensionality on the anisotropy was given. The dissipation coefficient γ_K influences the anisotropy A in the same manner as k_s: The increase of γ_K results in increase of A. This could be explained by using Eq. (21) for the relaxation time of K collective coordinate. The large γ_K value will result in faster relaxation

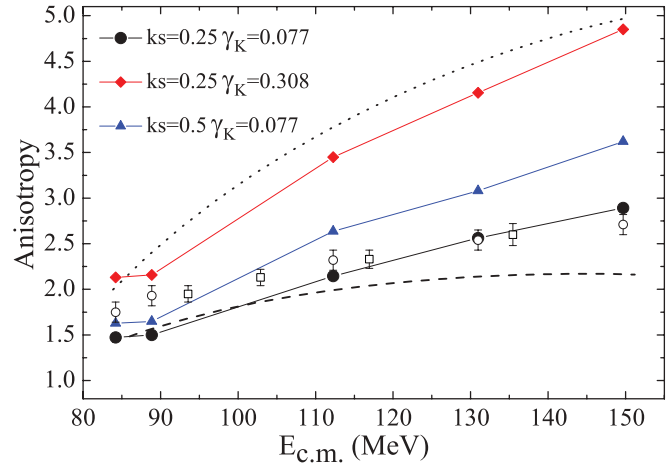

FIG. 11. (Color online) The anisotropy of the fission fragment angular distribution as a function of the center-of-mass energy for the reaction ^{16}O + ^{232}Th → ^{248}Cf. The calculated points are connected by lines to guide the eye. The open symbols are the experimental data: Ref. [72] (circles), Ref. [75] (squares). The filled symbols are the calculated results with different values of k_s and γ_K, which are marked in the same order as in Fig. 9. The dotted and dashed curves present the results predicted by the SCTS and SPTS models, respectively.

of the K coordinate and more narrow K distribution, which will correspond to the large A values as seen from Eq. (17).

The satisfactory description of the experimental A values for both reactions could be obtained with $k_s = 0.25$ and $\gamma_K = 0.077$(MeV zs)$^{-1/2}$. The value $k_s = 0.25$ provides also a reasonable description for the fission fragment MED parameters and prescission particles multiplicities, as seen in previous section. The value $\gamma_K = 0.077$ (MeV zs)$^{-1/2}$ has been obtained in Ref. [19] from estimates of K-coordinate dissipation strength for elongated shapes on the descent from

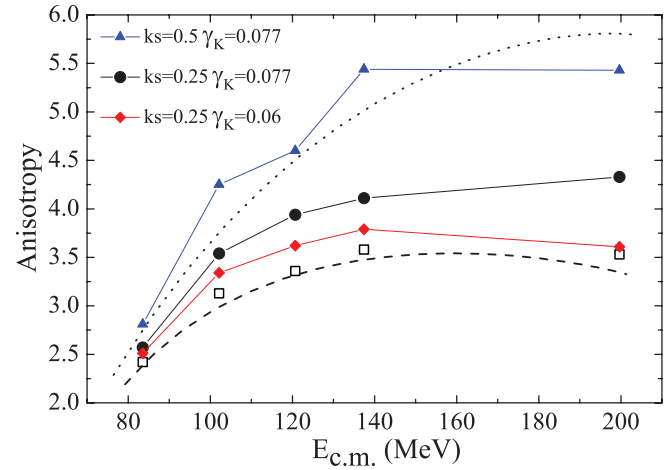

FIG. 12. (Color online) The anisotropy of the fission fragment angular distribution as a function of the center-of-mass energy for the reaction ^{16}O + ^{208}Pb → ^{224}Th. The calculated points are connected by lines to guide the eye. The open symbols are the experimental data [72,103]. The filled symbols are the calculated results with different values of k_s and γ_K, as in Fig. 6. The dotted and dashed curves present the results predicted by the SCTS and SPTS models, respectively.

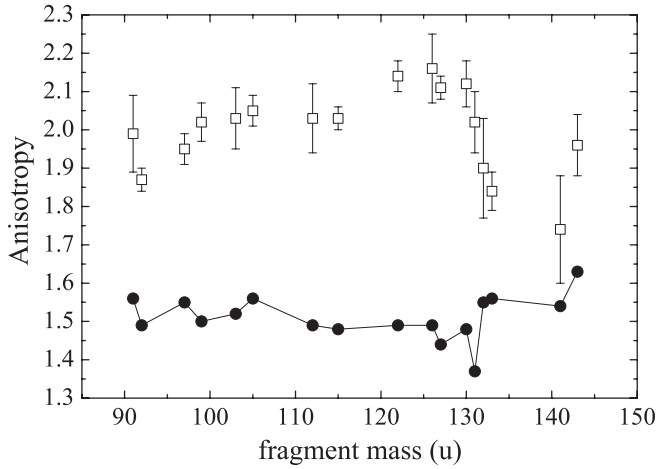

FIG. 13. The anisotropy of the angular distribution as a function of the fission fragment mass for the reaction $^{16}O + ^{232}Th \rightarrow ^{248}Cf$. The open squares are experimental data at $E_{lab} = 96$ MeV from Ref. [76], and the circles are calculated results at $E_{lab} = 95$ MeV with $k_s = 0.25$ and $\gamma_K = 0.077$ (MeV zs)$^{-1/2}$.

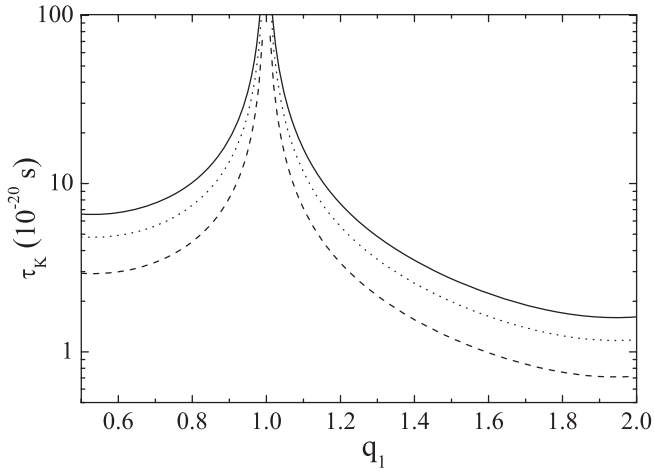

FIG. 14. The relaxation time of K coordinate τ_K as a function of the elongation parameter for the nucleus ^{224}Th obtained with Eq. (21). The solid curve is calculated at $\gamma_K = 0.077$ (MeV zs)$^{-1/2}$ and $I = 40$, the dashed curve at $\gamma_K = 0.077$ (MeV zs)$^{-1/2}$ and $I = 60$, and the dotted curve at $\gamma_K = 0.06$ (MeV zs)$^{-1/2}$ and $I = 60$.

saddle to scission point. Presently, we found that a value $\gamma_K \simeq 0.05$ (MeV zs)$^{-1/2}$ would be best suited for ^{224}Th at $E_{lab} = 110$ and 130 MeV, and $\gamma_K \simeq 0.2$(MeV zs)$^{-1/2}$ for ^{248}Cf at $E_{lab} = 90$ and 95 MeV. We made these estimations from the calculations presented in Figs. 11 and 12 assuming a smooth dependence of calculated anisotropy on the γ_K value. All these γ_K values are reasonable, as the estimation of $\gamma_K = 0.077$ (MeV zs)$^{-1/2}$ is quite rough [19]. The need for different γ_K values to reproduce experimental anisotropies could indicate the possible dependence of γ_K on the nuclear shape, as shown by Eq. (9) for a strongly necked in shapes. Another possible extension of the model would consist of taking into account the fission fragment spins at the scission point as discussed in Refs. [60,91–95]. Careful consideration of these effects in dynamical calculations may change the estimations of the γ_K value obtained in the present paper.

Available experimental data on the fission-fragment mass dependence of the anisotropy exist for the ^{248}Cf at $E_{lab} =$ 96 MeV [76]. The experimental data and theoretical estimations [96] both exhibit an independence of the anisotropy on the fission fragment mass as shown in Fig. 13. Although experimental values of the anisotropy are underestimated by about 25%, the qualitative independence of A on the fragment mass is reproduced in 4D calculations.

The relaxation time of the K coordinate τ_K is an important property of nuclear dynamics, which could be extracted from the present 4D calculations. Many investigations of the relaxation time in fusion-fission and quasifission reactions [20,22,52,61,62,97–102] predict a value of τ_K ranging from $\sim 10^{-21}$ s to $\sim 10^{-20}$ s depending on the spin, transition-state deformation, and type of the investigated reaction. The γ_K and I influence τ_K in a different way. The increase of γ_K increases the τ_K values. On the contrary, the increase of I decreases τ_K. The τ_K dependence on deformation and spin of compound nucleus predicted by Eq. (21) is presented in Fig. 14 for the nucleus ^{224}Th at different values of γ_K and I. The obtained τ_K values are in general agreement with previous estimations of $\tau_K \sim 10^{-20}$ s. The strong dependence of τ_K on deformation reflects the dependence of J_{eff} on the shape of the compound nucleus.

The typical values for the saddle to scission time τ_{ss} in our calculations are about (3–9) zs for ^{248}Cf and (1–5) zs for ^{224}Th, and they mostly depend on the friction parameter k_s. The τ_{ss} values become greater with increasing friction strength. As τ_K is comparable to τ_{ss}, the transition state would be located somewhere in between saddle and scission points. Moreover, in some cases the equilibrium K distribution may even not be achieved [104,105]. Qualitatively the dependence of calculated anisotropies on the excitation energy and friction parameters γ_K and k_s presented in Figs. 11 and 12 can be explained as follows. The increase of γ_K decreases the relaxation time of the K coordinate. Therefore, the effective transition state of K-distribution formation will be closer to the scission point, where larger values of fission fragment anisotropy are predicted. The increase of friction strength parameter k_s increases the number of evaporated prescission particles and, as a result, decreases the nuclear temperature. The decrease of temperature leads to a more narrow K distribution and larger A values as seen from Eqs. (14) and (17).

Comparing the present results of 4D calculations with 3D calculations [23,24], one can conclude that the additional collective coordinate K has substantial influence on the calculated MED characteristics and angular distribution of fission fragments. This coordinate increases the width of the mass distribution and prescission neutron multiplicity. Both effects help reproduce the experimental data on the fission fragment MED parameters together with the mean prescission neutron multiplicity for heavy fissioning nuclei more accurately.

IV. SUMMARY AND CONCLUSIONS

The four-dimensional dynamical model has been developed on the basis of the three-dimensional model [23–25] by adding

the orientation degree of freedom K to the three collective coordinates which describe the shape of the fissioning nucleus. It was found that the K degree of freedom not only increases fission barrier height, as reported before [19,77], but also changes the stiffness of the nucleus with respect to mass asymmetry coordinate $d^2F/d\eta^2$. The change of the stiffness results in a shift of the Businaro-Gallone point towards larger Z^2/A values. The Businaro-Gallone point moves from approximately $Z^2/A \simeq 20$ for the case of $K = 0$ to the $Z^2/A \simeq 25$ for the case of $L = K = 40$. The mass asymmetry stiffness $[d^2F(L, K)/d\eta^2]_{\rm sd}$ at the saddle point is significantly reduced with increase of K for the heavy nuclei with $Z^2/A \simeq 40$. The value of $[d^2F(L = 40, K = 40)/d\eta^2]_{\rm sd}$ is around 5 times lower than $[d^2F(L = 40, K = 0)/d\eta^2]_{\rm sd}$ at $Z^2/A = 40$.

The wide set of experimental data available for the reactions $^{16}{\rm O} + {}^{208}{\rm Pb} \rightarrow {}^{224}{\rm Th}$ and $^{16}{\rm O} + {}^{232}{\rm Th} \rightarrow {}^{248}{\rm Cf}$ has been analyzed using the new 4D dynamical model. The prescission neutron multiplicities, fission fragment MED parameters, and anisotropy of angular distribution could be reasonably reproduced for heavy nuclei with the dissipation coefficients $k_s \simeq 0.25$ and $\gamma_K \simeq 0.077$ (MeV zs)$^{-1/2}$ in contrast with 3D calculations [23,24], where a self-consistent description of all observables with the same k_s value was impossible for heavy nuclei. Reproduction of MED parameters in 3D calculations required small values of $k_s \simeq 0.1$, whereas $k_s \geqslant 1$ values are needed to reproduce prescission neutron multiplicities. Careful accounting of the influence of the K coordinate on the potential energy surface and on the dynamics of shape coordinates allows one to get a consistent picture of the fission process in 4D calculations. The present results show that taking the K coordinate into consideration would be preferable not only in statistical model calculations [17,19], but also in recent 5D dynamical studies [89,106,107].

The present 4D calculations demonstrate that the estimation of the dissipation coefficient for the K coordinate $\gamma_K \simeq 0.077$(MeV zs)$^{-1/2}$ made in Refs. [19,54] is reasonable and allows the reproduction of the anisotropy of the angular distribution for heavy fissioning nuclei. The obtained relaxation time of the K coordinate $\tau_K \sim 10^{-20}$ s is in agreement with previous studies.

ACKNOWLEDGMENTS

We would like to thank Dr. C. Schmitt for useful collaboration, discussions, and correspondence. We are grateful to Dr. D. O. Eremenko, Dr. A.V. Karpov, and Dr. G. I. Kosenko for their continued interest in this study and numerous enlightening stimulating discussions. We are also grateful to Larissa N. Hill for the careful reading of this manuscript. One of us (A.E.G.) is thankful to Omsk State University for the grant supporting this study.

[1] W. Ye, F. Wu, and H. W. Yang, Phys. Lett. B **647**, 118 (2007).
[2] W. Ye, Phys. Rev. C **80**, 011601 (2009).
[3] W. Ye, Phys. Rev. C **83**, 044611 (2011).
[4] G. Chaudhuri and S. Pal, Phys. Rev. C **65**, 054612 (2002).
[5] C. Schmitt, J. Bartel, K. Pomorski, and A. Surowiec, Acta Phys. Pol. B **34**, 1651 (2003).
[6] C. Schmitt, J. Bartel, A. Surowiec, and K. Pomorski, Acta Phys. Pol. B **34**, 2135 (2003).
[7] Y. Aritomo, J. Nucl. Radiochem. Sci. **3**, 17 (2002).
[8] G. I. Kosenko, F. A. Ivanyuk, and V. V. Pashkevich, J. Nucl. Radiochem. Sci. **3**, 71 (2002).
[9] I. I. Gontchar, A. E. Gettinger, L. V. Guryan, and W. Wagner, Phys. At. Nucl. **63**, 1688 (2000).
[10] P. N. Nadtochy, A. Kelić, and K.-H. Schmidt, Phys. Rev. C **75**, 064614 (2007).
[11] E. G. Ryabov, A. V. Karpov, P. N. Nadtochy, and G. D. Adeev, Phys. Rev. C **78**, 044614 (2008).
[12] P. N. Nadtochy, E. Vardaci, A. Di Nitto, A. Brondi, G. La Rana, R. Moro, M. Cinausero, G. Prete, N. Gelli, and F. Lucarelli, Phys. Lett. B **685**, 258 (2010).
[13] Y. Jia and J.-D. Bao, Phys. Rev. C **75**, 034601 (2007).
[14] S. Pal, G. Chaudhuri, and J. Sadhukhan, Nucl. Phys. A **808**, 1 (2008).
[15] J. Sadhukhan and S. Pal, Phys. Rev. C **84**, 044610 (2011).
[16] M. R. Pahlavani and D. Naderi, Phys. Rev. C **83**, 024602 (2011).
[17] J. P. Lestone, Phys. Rev. C **59**, 1540 (1999).
[18] S. G. McCalla and J. P. Lestone, Phys. Rev. Lett. **101**, 032702 (2008).
[19] J. P. Lestone and S. G. McCalla, Phys. Rev. C **79**, 044611 (2009).
[20] D. O. Eremenko, V. A. Drozdov, M. H. Eslamizadex, O. V. Fotina, S. Y. Platonov, and O. A. Yuminov, Phys. At. Nucl. **69**, 1423 (2006).
[21] A. V. Karpov, R. M. Hiryanov, A. V. Sagdeev, and G. D. Adeev, J. Phys. G: Nucl. Part. Phys. **34**, 255 (2007).
[22] R. M. Hiryanov, A. V. Karpov, and G. D. Adeev, Phys. At. Nucl. **71**, 1361 (2008).
[23] A. V. Karpov, P. N. Nadtochy, D. V. Vanin, and G. D. Adeev, Phys. Rev. C **63**, 054610 (2001).
[24] P. N. Nadtochy, G. D. Adeev, and A. V. Karpov, Phys. Rev. C **65**, 064615 (2002).
[25] G. D. Adeev, A. V. Karpov, P. N. Nadtochy, and D. V. Vanin, Fiz. Elem. Chast. At. Yadra **36**, 732 (2005).
[26] M. Brack, J. Damgaard, A. S. Jensen, H. C. Pauli, V. M. Strutinsky, and C. Y. Wong, Rev. Mod. Phys. **44**, 320 (1972).
[27] H. A. Kramers, Physica **7**, 284 (1940).
[28] H. J. Krappe, in *Proceedings of the XIII Meeting on Physics of Nuclear Fission in Memory of Prof. G. N. Smirenkin, Obninsk, 1995*, edited by B. D. Kuzminov (SSCRF-IPPE, Obninsk, 1995), pp. 134–144.
[29] Y. Abe, S. Ayik, P.-G. Reinhard, and E. Suraud, Phys. Rep. **275**, 49 (1996).
[30] P. Fröbrich and I. I. Gontchar, Phys. Rep. **292**, 131 (1998).
[31] A. Ignatyuk, M. G. Itkis, V. Okolovich, and G. Smirenkin, Yad. Fiz. **21**, 1185 (1975).
[32] P. N. Nadtochy and G. D. Adeev, Phys. Rev. C **72**, 054608 (2005).
[33] H. J. Krappe, J. R. Nix, and A. J. Sierk, Phys. Rev. C **20**, 992 (1979).

[34] A. J. Sierk, Phys. Rev. C **33**, 2039 (1986).
[35] K. T. R. Davies, A. J. Sierk, and J. R. Nix, Phys. Rev. C **13**, 2385 (1976).
[36] J. Blocki, Y. Boneh, J. R. Nix, J. Randrup, M. Robel, A. J. Sierk, and W. J. Swiatecki, Ann. Phys. (NY) **113**, 330 (1978).
[37] J. Randrup and W. J. Swiatecki, Ann. Phys. (NY) **125**, 193 (1980).
[38] J. R. Nix and A. J. Sierk, in *Proceedings of the International School-Seminar on Heavy Ion Physics, Dubna, USSR, 1986*, edited by M. I. Zarubina and E. V. Ivashkevich (JINR, Dubna, 1987), pp. 453–464.
[39] J. R. Nix and A. J. Sierk, in *Proceedings of the 6th Adriatic Conference on Nuclear Physics: Frontiers of Heavy Ion Physics, Dubrovnik, Yugoslavia, 1987*, edited by N. Cindro, R. Caplar, and W. Greiner (World Scientific, Singapore, 1990), pp. 333–340.
[40] J. Randrup and W. J. Swiatecki, Nucl. Phys. A **429**, 105 (1984).
[41] J. Blocki, H. Feldmeier, and W. Swiatecki, Nucl. Phys. A **459**, 145 (1986).
[42] P. N. Nadtochy, A. V. Karpov, and G. D. Adeev, Phys. At. Nucl. **65**, 799 (2002).
[43] T. Wada, Y. Abe, and N. Carjan, Phys. Rev. Lett. **70**, 3538 (1993).
[44] P. N. Nadtochy, A. V. Karpov, D. V. Vanin, and G. D. Adeev, Phys. At. Nucl. **66**, 1203 (2003).
[45] J. J. Griffin and M. Dworzecka, Nucl. Phys. A **455**, 61 (1986).
[46] S. Pal and T. Mukhopadhyay, Phys. Rev. C **54**, 1333 (1996).
[47] T. Mukhopadhyay and S. Pal, Phys. Rev. C **56**, 296 (1997).
[48] S. Pal and T. Mukhopadhyay, Phys. Rev. C **57**, 210 (1998).
[49] V. A. Drozdov, D. O. Eremenko, O. V. Fotina, S. Y. Platonov, and O. A. Yuminov, in *Tours Symposium on Nuclear Physics V, Tours 2003*, AIP Conf. Proc. Vol. 704, edited by M. Arnold, M. Lewitowicz, G. Münzenberg, H. Akimune, M. Ohta, H. Utsunomiya, T. Wada, and T. Yamagata (AIP, Melville, New York, 2004), pp. 130–138.
[50] K. T. R. Davies and J. R. Nix, Phys. Rev. C **14**, 1977 (1976).
[51] R. W. Hasse and W. D. Myers, *Geometrical Relationships of Macroscopic Nuclear Physics* (Springer-Verlag, Heidelberg, 1988), p. 116.
[52] T. Døssing and J. Randrup, Nucl. Phys. A **433**, 215 (1985).
[53] J. Randrup, Nucl. Phys. A **383**, 468 (1982).
[54] J. P. Lestone, A. A. Sonzogni, M. P. Kelly, and R. Vandenbosch, J. Phys. G: Nucl. Part. Phys. **23**, 1349 (1997).
[55] N. D. Mavlitov, P. Fröbrich, and I. I. Gontchar, Z. Phys. A **342**, 195 (1992).
[56] J. Marten and P. Fröbrich, Nucl. Phys. A **545**, 854 (1992).
[57] K. T. R. Davies, R. A. Managan, J. R. Nix, and A. J. Sierk, Phys. Rev. C **16**, 1890 (1977).
[58] R. Vandenbosch and J. R. Huizenga, *Nuclear Fission* (New York, Academic Press, 1973), p. 424.
[59] A. Bohr and B. R. Mottelson, *Nuclear Structure*, Vol. 2 (World Scientific, Singapore, 1998), p. 748.
[60] H. H. Rossner, J. R. Huizenga, and W. U. Schröder, Phys. Rev. Lett. **53**, 38 (1984).
[61] D. O. Eremenko, A. A. Dermenev, V. A. Drozdov, S. Y. Platonov, O. V. Fotina, and O. A. Yuminov, Bull. Rus. Acad. Sci., Phys. **73**, 180 (2009).
[62] J. Randrup and T. Døssing, Nucl. Phys. A **428**, 255 (1984).
[63] C. R. Morton, D. J. Hinde, J. R. Leigh, J. P. Lestone, M. Dasgupta, J. C. Mein, J. O. Newton, and H. Timmers, Phys. Rev. C **52**, 243 (1995).
[64] K.-T. Brinkmann, A. L. Caraley, B. J. Fineman, N. Gan, J. Velkovska, and R. L. McGrath, Phys. Rev. C **50**, 309 (1994).
[65] T. Murakami, C.-C. Sahm, R. Vandenbosch, D. D. Leach, A. Ray, and M. J. Murphy, Phys. Rev. C **34**, 1353 (1986).
[66] F. Videbaek, R. B. Goldstein, L. Grodzins, and S. G. Steadman, Phys. Rev. C **15**, 954 (1977).
[67] M. Dasgupta, D. J. Hinde, A. Diaz-Torres, B. Bouriquet, C. I. Low, G. J. Milburn, and J. O. Newton, Phys. Rev. Lett. **99**, 192701 (2007).
[68] E. Vulgaris, L. Grodzins, S. G. Steadman, and R. Ledoux, Phys. Rev. C **33**, 2017 (1986).
[69] E. Vulgaris, L. Grodzins, S. G. Steadman, and R. Ledoux, Phys. Rev. C **34**, 1495(E) (1986).
[70] M. G. Itkis, Y. T. Oganessian, G. G. Chubarian, V. S. Salamatin, A. Y. Rusanov, and V. N. Okolovich, in *Proceedings of the EPS XV Nuclear Physics Divisional Conference on Low Energy Nuclear Dynamics (LEND-95), St Petersburg, Russia, April, 1995*, edited by Y. T. Oganessian, R. Kalpakchieva, and W. von Oertzen (World Scientific, Singapore, 1995), pp. 177–180.
[71] H. H. Rossner, D. J. Hinde, J. R. Leigh, J. P. Lestone, J. O. Newton, J. X. Wei, and S. Elfström, Phys. Rev. C **45**, 719 (1992).
[72] B. B. Back, R. R. Betts, J. E. Gindler, B. D. Wilkins, S. Saini, M. B. Tsang, C. K. Gelbke, W. G. Lynch, M. A. McMahan, and P. A. Baisden, Phys. Rev. C **32**, 195 (1985).
[73] M. G. Itkis, S. M. Lukyanov, V. N. Okolovich, Y. E. Penionzkevich, A. Y. Rusanov, V. S. Salamatin, G. N. Smirenkin, and G. G. Chubaryan, Phys. At. Nucl. **52**, 15 (1990).
[74] A. Saxena, A. Chatterjee, R. K. Choudhury, S. S. Kapoor, and D. M. Nadkarni, Phys. Rev. C **49**, 932 (1994).
[75] S. Kailas, D. M. Nadkarni, A. Chatterjee, A. Saxena, S. S. Kapoor, R. Vandenbosch, J. P. Lestone, J. F. Liang, D. J. Prindle, A. A. Sonzogni, and J. D. Bierman, Phys. Rev. C **59**, 2580 (1999).
[76] B. John, A. Nijasure, S. K. Kataria, A. Goswami, B. S. Tomar, A. V. R. Reddy, and S. B. Manohar, Phys. Rev. C **51**, 165 (1995).
[77] M. Prakash, V. S. Ramamurthy, S. S. Kapoor, and J. M. Alexander, Phys. Rev. Lett. **52**, 990 (1984).
[78] V. M. Strutinsky, Zh. Eksp. Teor. Fiz. **45**, 1891 (1963).
[79] M. G. Itkis and A. Y. Rusanov, Phys. Part. Nucl. **29**, 160 (1998).
[80] Y. A. Anischenko, A. E. Gegechkori, and G. D. Adeev, Act. Phys. Pol. B **42**, 493 (2011).
[81] Y. A. Anischenko, A. E. Gegechkori, P. N. Nadtochy, and G. D. Adeev, in *International Symposium on Exotic Nuclei, Sochi, Russia, 2009*, AIP Conf. Proc. Vol. 1224, edited by Y. E. Penionzhkevich and S. M. Lukyanov (AIP, New York, 2010), pp. 350–355.
[82] Y. A. Anischenko, A. E. Gegechkori, P. N. Nadtochy, and G. D. Adeev, Phys. At. Nucl. **72**, 1992 (2009).
[83] P. Fröbrich and H. Rossner, Z. Phys. A **349**, 99 (1994).
[84] J. Wilczyński, K. Siwek-Wilczyńska, and H. W. Wilschut, Phys. Rev. C **54**, 325 (1996).
[85] K. Mazurek, C. Schmitt, J. P. Wieleczko, P. N. Nadtochy, and G. Ademard, Phys. Rev. C **84**, 014610 (2011).
[86] M. Borunov, P. Nadtochy, and G. Adeev, Nucl. Phys. A **799**, 56 (2008).
[87] G. D. Adeev and P. N. Nadtochy, Phys. At. Nucl. **66**, 618 (2003).
[88] P. Möller, A. J. Sierk, T. Ichikawa, A. Iwamoto, R. Bengtsson, H. Uhrenholt, and S. Åberg, Phys. Rev. C **79**, 064304 (2009).
[89] J. Randrup and P. Möller, Phys. Rev. Lett. **106**, 132503 (2011).

[90] V. Pashkevich and A. Rusanov, Nucl. Phys. A **810**, 77 (2008).
[91] P. D. Bond, Phys. Rev. Lett. **52**, 414 (1984).
[92] P. D. Bond, Phys. Rev. C **32**, 471 (1985).
[93] H. Rossner, J. R. Huizenga, and W. U. Schröder, Phys. Rev. C **33**, 560 (1986).
[94] B. John and S. K. Kataria, Phys. Rev. C **57**, 1337 (1998).
[95] A. Y. Rusanov, G. D. Adeev, M. G. Itkis, A. V. Karpov, P. N. Nadtochy, V. V. Pashkevich, I. V. Pokrovsky, V. S. Salamatin, and G. G. Chubarian, Phys. At. Nucl. **70**, 1679 (2007).
[96] D. De Frenne, *The Nuclear Fission Process*, edited by C. Wagemans (CRC Press, Boca Raton, FL, 1991), Chap. 9, pp. 475–491.
[97] T. Døssing and J. Randrup, Nucl. Phys. A **433**, 280 (1985).
[98] T. Døssing and J. Randrup, Phys. Lett. B **155**, 333 (1985).
[99] K. Lützenkirchen, J. V. Kratz, G. Wirth, W. Brüchle, K. Sümmerer, R. Lucas, J. Poitou, and C. Grégoire, Nucl. Phys. A **452**, 351 (1986).
[100] R. G. Thomas, R. K. Choudhury, A. K. Mohanty, A. Saxena, and S. S. Kapoor, Phys. Rev. C **67**, 041601 (2003).
[101] M. A. Butler, S. S. Datta, R. T. de Souza, J. R. Huizenga, W. U. Schröder, J. Töke, and J. L. Wile, Phys. Rev. C **34**, 2016 (1986).
[102] V. A. Drozdov, D. O. Eremenko, O. V. Fotina, G. Giardina, F. Malaguti, S. Y. Platonov, and O. A. Yuminov, Nucl. Phys. A **734**, 225 (2004).
[103] L. C. Vaz, D. Logan, E. Duek, J. M. Alexander, M. F. Rivet, M. S. Zisman, M. Kaplan, and J. W. Ball, Z. Phys. A **315**, 169 (1984).
[104] J. M. Alexander, Ann. Phys. (Paris) **12**, 603 (1987).
[105] R. Freifelder, M. Prakash, and J. M. Alexander, Phys. Rep. **133**, 315 (1986).
[106] J. Randrup, P. Möller, and A. J. Sierk, Phys. Rev. C **84**, 034613 (2011).
[107] P. Möller, J. Randrup, and A. J. Sierk, Phys. Rev. C **85**, 024306 (2012).